

Article

Research on the Efficient Space Debris Observation Method Based on Optical Satellite Constellations

Gongqiang Li ^{1,2,3,*}, Jing Liu ^{1,2,3}, Hai Jiang ^{2,3}  and Chengzhi Liu ^{1,2}

¹ Changchun Observatory, National Astronomical Observatories, Chinese Academy of Sciences, Changchun 130117, China

² University of Chinese Academy of Sciences, Beijing 100049, China

³ National Astronomical Observatories, Chinese Academy of Sciences, Beijing 100101, China

* Correspondence: ligongqiang@bao.ac.cn

Abstract: The increasing amount of space debris poses a major threat to the security of space assets. The timely acquisition of space debris orbital data through observations is essential. We established a mathematical model of optical satellite constellations for space debris observation, designed a high-quality constellation configuration, and designed a space debris tracking observation scheduling algorithm. These tools can realize the efficient networking of space debris from a large number of optical satellite observation facilities. We designed a constellation consisting of more than 20 low-Earth orbit (LEO) satellites, mainly dedicated to the observation of LEO space objects. According to the observation scheduling method, the satellite constellation can track and observe more than 93% of the targets every day, increase the frequency of orbital data updates, and provide support for the realization of orbital space debris cataloguing. Designing optical satellite constellations to observe space debris can help realize the advance perception of dangerous collisions, timely detect dangerous space events, make key observations about high-risk targets, greatly reduce the false alarm rate of collisions, and provide observational data support for space collisions.

Keywords: constellation; satellite; observation; space debris; scheduling



Citation: Li, G.; Liu, J.; Jiang, H.; Liu, C. Research on the Efficient Space Debris Observation Method Based on Optical Satellite Constellations. *Appl. Sci.* **2023**, *13*, 4127. <https://doi.org/10.3390/app13074127>

Academic Editors: Lorenzo Olivieri, Kanjuro Makihara and Leonardo Barilaro

Received: 16 February 2023

Revised: 7 March 2023

Accepted: 20 March 2023

Published: 24 March 2023



Copyright: © 2023 by the authors. Licensee MDPI, Basel, Switzerland. This article is an open access article distributed under the terms and conditions of the Creative Commons Attribution (CC BY) license (<https://creativecommons.org/licenses/by/4.0/>).

1. Introduction

Space debris refers to the non-functional man-made objects in orbit. Human space activities have a history of more than 60 years, and it is estimated that there are over 30,000 pieces of debris larger than 10 cm, approx. one million pieces of debris larger than 1 cm, and hundreds of millions of millimeter-level space debris. Space debris and spacecraft move around the Earth at a high speed of more than 7.9 km/s, and the relative speed of space debris can reach more than 10 km/s when a collision occurs. The impact of a 1 cm-sized aluminum ball in space will produce a destructive force equivalent to the impact of a car on the highway. The consequences of the impacts of space debris above 1 cm are often devastating, and large-sized space debris above 10 cm will directly lead to spacecraft failure [1–3]. Space collisions have become more frequent in recent years. In 2019, there were more than 300 dangerous impacts between Chinese spacecraft in orbit and space debris. In 2013, the Ecuadorian CubeSats collided with Soviet rocket debris, causing the satellite to fail. On 12 June 2011, the solar cells of the IGSO-2 satellite of China's Beidou navigation constellation lost two circuits, and the conclusion confirmed that the satellite was hit by small debris. On 11 February 2009, the US commercial communications satellite Iridium-33 collided with Russia's abandoned Cosmos-2251 satellite, with a relative speed of 11.6 km per second, generating more than 2000 pieces of space debris, which caused strong repercussions from the international community [4].

With the development of human space activities, the number of space objects is increasing. At the same time, the development of large satellite constellations and the competition for space interests of various countries have made the space situation increasingly

complex [5]. This poses a major threat to the security of space activities and space assets. It is necessary to obtain the orbit information of space objects in real time to meet the demand for accurately detecting space events [6]. Monitoring space objects using monitoring equipment and optimizing the scheduling of the monitoring system is an effective way to obtain the space object's status information [7]. By adopting efficient observation scheduling methods, the number of space objects and arcs observed by observation equipment in a certain period can be increased, and the observation efficiency can be improved [8].

Compared to traditional ground-based optical telescopes, space-based optical satellites have unique advantages because they run in orbit and their detection of space objects are not affected by the weather. In addition, the detector is closer to the space object, and an optical telescope with a smaller aperture can be used to observe the low-orbit space target at a shorter distance. Most space-based satellite constellations are deployed in low Earth orbit where space debris is mainly distributed. Therefore, satellite constellations can fully observe the low Earth orbit airspace where space objects are densely distributed, improve the detection quantity and frequency of space objects, make full use of space detection equipment, obtain a large amount of observation data in real time, realize the dynamic catalogue of space debris, provide early warning of dangerous collisions, and maintain the order of space traffic and the safety of space assets [9].

Reasonable monitoring task scheduling is the key for the effective operation of a space-based monitoring network. Especially due to the development of various space-based monitoring equipment and the improvement of the automation of observation equipment, new requirements have been put forward to optimize observation task scheduling. Space object observation scheduling optimization is bound to be closely related to the specific situation of equipment operation and the movement of the space object itself. Special research needs to be conducted on the specific application observation mode and the equipment operation state. This is a very complex combinatorial optimization problem that exhibits multi-time window constraints, multi-resource constraints, and high conflict, and it has become one of the leading issues in the field of space monitoring [10–12].

The current observation scheduling algorithm is not suitable for rapidly moving observation equipment and observation targets, and there is little research on the observation task scheduling of space-based satellite constellations. The research on the observation task scheduling algorithm of space-based optical satellite detecting for space objects is the key for improving the efficiency of space object detection, and it is also one of the important problems that needs to be solved in the field of space object observation [13–15].

We designed satellite constellations with different configurations and created a constellation observation task scheduling algorithm. The main purpose was to track and observe LEO space objects, obtain a large amount of observation data, and update the object orbit information in real time. The goal was to catalog a large number of LEO space objects using a constellation composed of a small number of satellites. The space objects orbit data were used for the simulation and verification, and good results were obtained. With the observation of satellite constellation, we can realize space situation awareness, provide emergency response to space emergencies, reduce collision risks, and maintain the safety of space assets.

2. Constellation Design

2.1. Model Establishment

The constellation spatial coverage model was established by comprehensively considering the point coverage numerical simulation model, the optical sensor coverage calculation, ground shadow model, the visual function, and the constellation comprehensive coverage performance evaluation index [16]. The point coverage numerical simulation technology was used to divide the target airspace into multiple blocks according to specific criteria. According to the constellation coverage of all the blocks, the space and time coverage performance of the constellation to the target airspace was analyzed. In order to avoid the infrared radiation interference of the Earth and its atmosphere, the optical sensors on

the satellite could only face the cold background of the universe to detect space objects above the edge of the Earth. The influence of the Earth's shadow on the observation of space debris also needs to be considered. The coverage of the constellation to the target airspace was measured in time and space to evaluate the comprehensive coverage performance of the constellation.

(1) Point coverage numerical simulation model

The numerical simulation technique of the point coverage is also known as the spatial meshing method [17], as shown in Figure 1. The target airspace is divided into grid points according to specific criteria, and the coverage of the target airspace in time and space is analyzed according to the coverage of all the airspace grid points by the constellation.

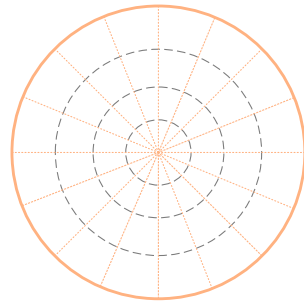


Figure 1. Schematic diagram of the point coverage grid method.

The problem surrounding constellation coverage in general Earth observation is that it mainly considers the two-dimensional coverage of the earth's surface. Due to the need to monitor space debris, two-dimensional grid point sampling needs to be extended to three-dimensional, and low-orbit space-based optical satellite constellations need to consider three-dimensional coverage within a certain altitude range above the Earth's surface where the sampled airspace is roughly a spherical shell. To establish a three-dimensional grid point sampling criterion, the height variables and the sample latitude, longitude, and altitude at the intervals need to be added.

(2) Optical sensor coverage calculation

In order to avoid infrared radiation interference from the Earth and its atmosphere, the optical sensor of the satellite can only be oriented towards the cosmic cold background of space to detect objects above the edge of the Earth [18], as shown in Figure 2.

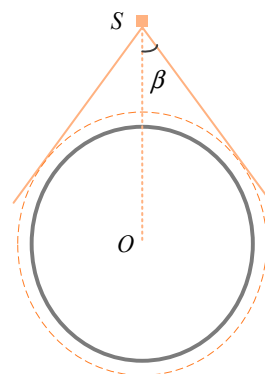


Figure 2. Coverage area of the space-based optical sensor.

In Figure 2, O is the center of the earth and S is the space-borne optical sensor. The solid circle represents the sphere model of the Earth, and the dotted circle represents the edge of the Earth's atmosphere. The sensor covers a sector beyond the tangent line of the satellite to the Earth's atmosphere.

The covering conditions of a space-based optical sensor for specific space debris in a specific altitude are shown in Formula (1).

$$\begin{cases} \varphi > \beta \\ 0 < d_{st} < L_{\max} \end{cases} \quad (1)$$

where φ is the angle between the space object and the Earth’s center relative to the satellite, β is the angle between the earth’s atmosphere boundary and the Earth’s center relative to the satellite, d_{st} is the distances between the satellites and the space object, and L_{\max} is the maximal detection range of the satellite-borne optical sensor.

(3) Earth shadow model

When space-based optical sensors observe space objects, the space objects need to be illuminated by the Sun. When the space object is in the shadowed area, the optical sensor cannot observe it, so the influence of the shadow on the observation of the space object needs to be considered.

Since the Sun is far from the Earth, the solar beam is regarded as parallel light and the sunlight that is obscured by the Earth produces a cylindrical shadow [19], as shown in Figure 3.

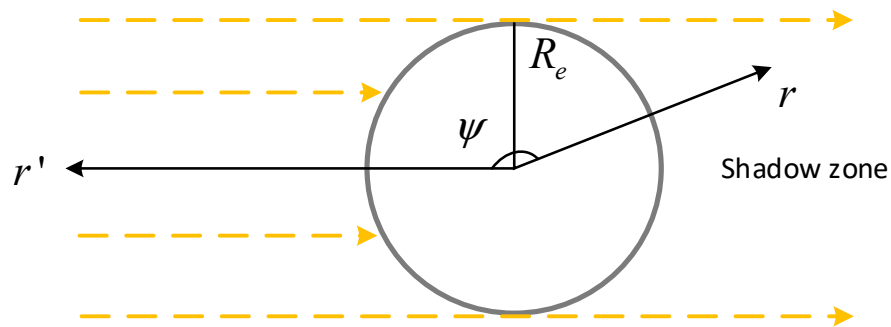


Figure 3. Cylindrical shadow model.

The following formula can be used to discover whether the grid point is in the shadow of the Earth. Satellites are not visible to space objects when they are in the Earth’s shadow zone, and satellites are visible to space objects when they are not in the Earth shadow zone. The value of the cylindrical shadow factor is -1 when the space object is in the shadow zone, otherwise it is 1 .

$$\begin{cases} -1, \psi > \frac{\pi}{2} \ \& \ r < \frac{R_e}{\sin \psi} \\ 1, \text{else} \end{cases} \quad (2)$$

where r is the connection between the grid points and the center of the earth, r' is the connection between the Sun and the center of the Earth, and ψ is the angle between r and r' . The angle ψ can be expressed using the following formula.

$$\cos \psi = \sin \delta_{sun} \sin \delta_{obj} + \cos \delta_{sun} \cos \delta_{obj} \cos(\alpha_{obj} - \alpha_{sun}) \quad (3)$$

where α_{sun} and δ_{sun} are the right ascension and declination of the Sun, α_{obj} and δ_{obj} are the right ascension and declination of the space objects. The position of the Sun changes with the seasons, so it is necessary to obtain multiple coordinate positions of the Sun, calculate the constellation’s space coverage performance for each position and identify the average. You can get the average coverage performance of the constellation in a year. In this model, the four positions of the Sun at the spring equinox ($0^\circ, 0^\circ$), the summer solstice ($90^\circ, 23^\circ 26'$), the autumnal equinox ($180^\circ, 0^\circ$), and the winter solstice ($270^\circ, -23^\circ 26'$) were taken to calculate the observation performance of the space objects by the constellations at different positions of the Sun.

(4) Visibility function

Define the visual function of F: When the sensor is visible to the grid points, $F > 0$ is the opposite of $F < 0$. The sub-apparent function is defined by the two conditions of Formula (1), respectively.

Define the visibility function of F: When the sensor is visible to the grid points, $F > 0$, and vice versa $F < 0$. According to the two conditions in Formula (1), the sub-visibility functions are defined separately as shown in the following formula [20].

$$f_1 = \varphi - \beta \tag{4}$$

$$f_2 = \frac{L_{\max} - d_{st}}{L_{\max}} \tag{5}$$

Define another sub-visibility function based on the Earth’s shadow condition as shown in the following formula.

$$f_3 = \begin{cases} -1, \Psi > \frac{\pi}{2} \&r < \frac{R_e}{\sin \Psi} \\ 1, \text{else} \end{cases} \tag{6}$$

It can be seen that when the values of the three Formulas (4)–(6) are greater than zero at the same time, the satellite can observe the grid point.

Define the visibility function as the following.

$$F = \min\{\text{sign}(f_1), \text{sign}(f_2), \text{sign}(f_3)\} \tag{7}$$

Define the visibility for each grid area as its visual value, denoted by C_j , which is 1 if the satellites are visible to the grid, otherwise it is 0. The visual value of each grid can be calculated using Formula (8).

$$C_j = \begin{cases} 1, (F > 0) \\ 0, (F < 0) \end{cases} \tag{8}$$

Visual value calculation rules of the grid: When the same grid can be detected by one satellite in the simulation time, the visual value of the satellite to the grid point is 1. When it is detected by the second satellite, the visual value is 1/2, and so on. When it is detected by the n -th satellite, the visual value is $1/n$.

(5) Constellation period calculation

For a specific grid area, the time interval between the recurrence of the corresponding satellite constellation geometry is the coverage period of the constellation to the grid area, and the smallest repeat interval is called the minimum coverage recurrence period.

The constellation period is calculated as follows.

$$T_C = \frac{T_s P}{T} \tag{9}$$

where $T_s = 2\pi\sqrt{\frac{a^3}{\mu}}$, T_C is the constellation period, T_s is the satellite period, and μ is the Earth’s gravity parameter. Here, the value is 398,600.4.

2.2. Theoretical Analysis

The constellation design was based on the walker- δ constellation [21,22]. All the satellite orbits in the constellation were circular orbits, with the same orbital altitude and inclination. The right ascension of all the orbital planes were evenly distributed. Through the establishment of the constellation airspace coverage model, using the appropriate objective functions and constraint conditions and optimizing the design using the genetic algorithm, the best constellation parameters that met the requirements were obtained, and the constellation configuration was determined. This constellation design mainly considered the coverage of the airspace in the orbital altitude range of 300–1000 km.

The assessment of the constellation’s coverage performance in the target airspace was measured in terms of time and space. At the same time, the distribution density of space objects in the grid area corresponding to different right ascensions, declinations, and altitudes in the airspace was considered, as shown in Figure 4. The resulting comprehensive coverage of the constellation was the ratio of the statistical sum of the volume, time, and density of all the observable grids of the constellation to the corresponding total.

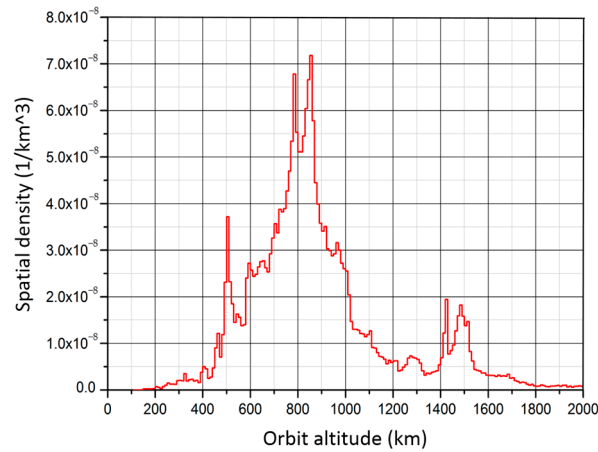


Figure 4. Distribution density of the space objects at different orbital altitudes.

The comprehensive coverage performance of the constellation can be expressed by the following formula, which is also used as the objective function of the constellation’s optimization design.

$$M_s = \frac{\sum_{j=1}^s (\rho_j V_j \sum_{l=1}^{T_C} d_t C_j)}{\sum_{j=1}^s \rho_j V_j T_C} \tag{10}$$

In the above formula, ρ_j is the spatial debris density corresponding to each grid area, V_j is the volume of each grid area, d_t is the simulation time step, C_j is the apparent value of each grid, S is the total number of grids, T is the number of satellites in the constellation, and T_C is the constellation period.

The constraints are as follows.

$$\begin{aligned} 12 < T < 24, \quad 3 \leq P \leq 6, \quad F = 1 \\ 0 \leq i \leq \pi, \quad 300 \text{ km} \leq a - R_e \leq 1000 \text{ km} \\ 0 \leq \Omega_0, \Omega_m \leq 2\pi, \quad 0 \leq M_{0,0}, M_{m,n} \leq 2\pi \end{aligned} \tag{11}$$

Finally, the constellation configuration and its parameters were determined as the following parameters: $T/P/F, a, i, \Omega_1, M_{1,1}$.

Here, T is the number of satellites in the constellation, P is the orbital plane number of the constellation, F is the phase factor, a is the orbital radius of the satellite, i is the orbital inclination, Ω_1 is the right ascension of the ascending nodes of the fiducial satellite in the constellation, $M_{1,1}$ is the mean anomaly of the fiducial satellite, and R_e is the earth radius.

According to the walker- δ constellation configuration, the positions of the satellites in the constellation can be represented by the following formula [23].

$$\begin{cases} \Omega_m = \Omega_1 + (m - 1) \frac{360}{P} \\ M_{m,n} = M_{1,1} + (m - 1) F \frac{360}{T} + (n - 1) P \frac{360}{T} \end{cases} \tag{12}$$

Here, Ω_m is the right ascension of the ascending nodes of the m -th orbital plane in the constellation and $1 \leq M \leq P$, $M_{m,n}$ is the mean anomaly of the n -th satellite on the m -th orbital plane, $1 \leq n \leq \frac{T}{P}$.

2.3. Design Results

We established the above constellation design model and optimized it using the genetic algorithms [24,25]. Then the optimal orbit parameters such as orbit altitude and inclination were obtained. According to these orbit parameters, the different constellation configurations were designed, and the spatial and time domain coverage performances of the constellations were analyzed according to the established model to obtain high-quality constellation configurations using screening.

The optimization process was carried out using the genetic algorithm, and the optimization process is shown in Figure 5. It can be seen from the figure that when the population evolved to 55 generations, the optimal solution can be obtained. The optimal orbital altitude was 609.782 km and the inclination angle was 96.142° .

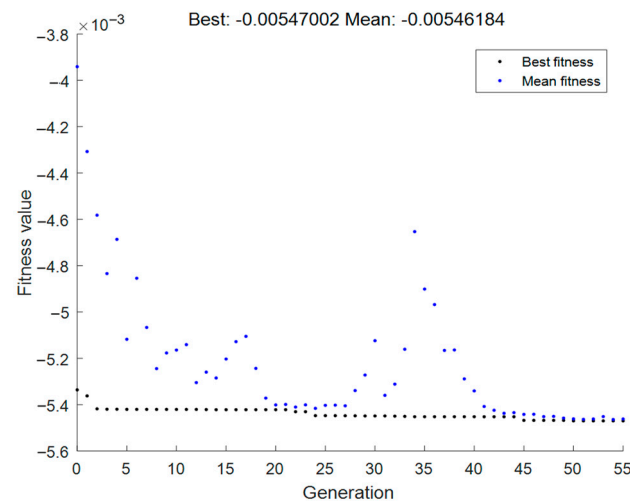


Figure 5. The optimization process of the orbital parameter design using the genetic algorithm.

The following situations were mainly considered, namely the number of orbital planes ($P = 3, 4, 5, 6$) And the number of constellation satellites ($T = 12, 15, 16, 18, 20, 21, 24$). Corresponding to the following 13 constellation configurations (12_3P, 12_4P, 12_6P, 15_3P, 15_5P, 16_4P, 18_3P, 18_6P, 20_5P, 21_3P, 24_3P, 24_4P, 24_6P), the specific meaning was that, taking 18_3P as an example, the constellation was composed of 18 satellites that were evenly distributed on three orbital planes, with six satellites on each orbital plane. The right ascension of each orbital plane was evenly distributed and the angle between the adjacent orbital planes was 120° .

According to the optimal deployment orbit altitude and the inclination of the satellite, and then according to the constellation spatial coverage model established above, the spatial coverage performance of each constellation can be calculated to judge the quality of the constellation's monitoring performance.

The calculated airspace coverage performance of each constellation is shown in Figure 6. The airspace coverage performance represents the airspace performance indicators that can be covered by all the different constellations in a constellation cycle, which can be used to compare the performance of each constellation. It can be seen from the figure that with the increase in the number of satellites in the constellation, the airspace coverage performance of the constellation showed an upward trend as a whole. However, the constellation with the same number of satellites had a very different performance due to the different constellation configurations. Therefore, the reasonable design of the constellation configuration plays a very important role for improving the observation efficiency of the constellation.

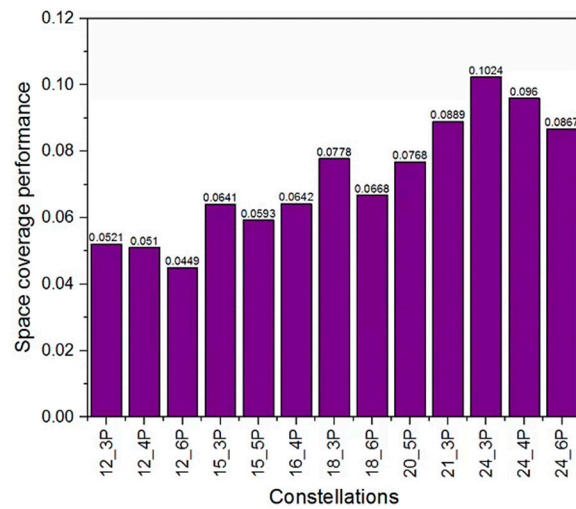


Figure 6. The airspace coverage performance of each constellation.

3. Constellation Observation Optimal Scheduling

3.1. Overview of Task Scheduling

Due to the large number of space objects [26], as shown in Figure 7, the space-borne optical telescope can only track one space object at a time. In order for the satellite constellation to monitor space debris during all weather events and at all times and achieve multi-satellite coordination, make full use of space-based observation equipment resources, reduce inefficient repeated observation, and improve the observation efficiency, it is necessary to develop an optimal scheduling algorithm for the observation tasks of space-based satellite constellations. This includes formulating efficient observation plans for each satellite and improve the monitoring efficiency.

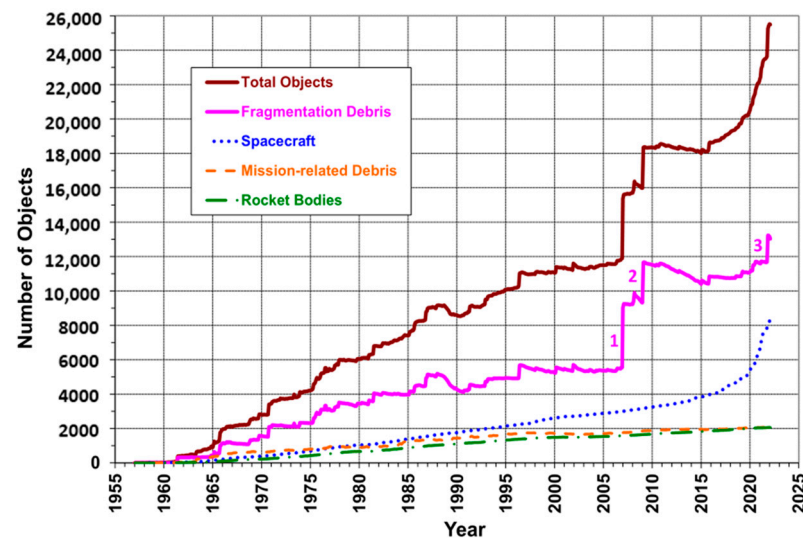


Figure 7. Growth trend in the number of space objects.

The goal of space-based observation equipment detection task scheduling is to allocate detection resources to significantly improve the detection and prediction capabilities for space objects to a certain extent. This allocation must consider many influencing factors, such as the observation capability of each sensor, the orbit accuracy of each observation object, and the detection frequency required to maintain a catalog of space objects. Space-based optical satellite observation task scheduling is a combined optimization problem under complex constraints. Its observation equipment and observation targets move at high speeds; it exhibits multi-time window constraints, multi-resource constraints, and

high conflicts; and it has become one of the leading issues in the field of space observation. When the amount of observation equipment and targets increases, the complexity of the optimization problem will increase geometrically.

3.2. Principles of Observation Task Scheduling

Each detection device has its own independent requirements and tasks. Task scheduling is to allocate time for each device to observe the space objects every day. In brief, the satellite network observation task scheduling problem refers to scheduling different satellite observation equipment to observe space objects in the observable time period under certain constraints [27,28]. That is, the detection scheduling result is better under certain expected effects (such as the largest number of observation targets and the highest equipment utilization).

The principle of task optimization scheduling is to track as many space objects as possible [29]. At the same time, the turning angle of the telescope should be made smaller and the idle time of the telescope should be minimized. Observation is given to objects with high priority and the space objects with short arcs are observed first. The objects with small phase angles are also observed first, followed by the targets with small changes, etc.

Suppose there are a total of N space objects to be observed. For any space object $n \in \{1, \dots, N\}$, the space object is divided into R classes, and the level of each space object is expressed as $l_n, l_n \in \{1, \dots, R\}$. Each space object can only be observed within a time window, expressed as $[O_n, D_n]$, where O_n is the initial time when the space object can be observed and D_n is the cut-off time.

Suppose there are a total of M optical observation satellites, for which any satellite $m \in \{1, \dots, M\}$. An optical satellite can observe only one space object at a time, and likewise, each space object can only be assigned to one optical satellite for observation. The definition of the $(0, 1)$ variables $x_{n,m}$, $x_{n,m} = 1$ indicates that the space object to be observed n is assigned to the optical satellite m , otherwise $x_{n,m} = 0$. The observation start time of the space object n is S_n and the observation end time is C_n , which is expressed as the following formula.

$$C_n = \begin{cases} S_n + t_{\min}, & \text{if } D_n - S_n \geq t_{\min} \\ D_n, & \text{Otherwise} \end{cases} \quad (13)$$

From S_n and C_n , the observation time P_n can be calculated as the following.

$$P_n = C_n - S_n \quad (14)$$

The time it takes for an optical satellite to observe a space object must be $\geq t_{\min}$ seconds to be counted as a successful observation. The observation result k_n of the space object n is expressed as the following.

$$k_n = \begin{cases} 1, & P_n \geq t_{\min} \\ 0, & \text{Otherwise} \end{cases} \quad (15)$$

where k_n is the $(0, 1)$ variable, $k_n = 1$ indicates that the observation of the space object n is successful, and $k_n = 0$ indicates that the observation failed.

In order to observe as many high-priority space objects as possible, the purpose of observation scheduling is the total weighted number K_{NL} of successful observations of space objects, which can be expressed as the following.

$$K_{NL} = \sum_{n=1}^N \sum_{m=1}^M x_{n,m} \cdot k_n \cdot l_n \quad (16)$$

Therefore, the constellation observation scheduling model is established as follows.

$$\max K_{NL} = \sum_{n=1}^N \sum_{m=1}^M x_{n,m} \cdot k_n \cdot l_n \quad (17)$$

The greedy algorithm based on the multi-dimensional list is used for constellation observation task scheduling, and the algorithm is introduced below.

(a) Algorithm Fundamentals

The multi-dimensional dynamic list programming algorithm is a fast heuristic approach for solving the match between the tasks and resources. It is a combination of a set of algorithms, which can be roughly divided into two parts, namely [30,31]:

- (1) To determine the priority function of the task.
- (2) To determine the priority function of the observation platform.

Among them, the priority function of the observation task is used to clarify that the task needs to be processed and is selected according to the task priority. The priority is selected first, and the subtask execution order is also arranged according to the size of the priority, from largest to smallest, with the large task executed first and the small task executed later. Determining the priority of the satellite platform selection dynamically identifies the priority of each current idle platform according to the platform resource priority function. From all the priority values obtained by all idle platforms, the highest priority is selected first and the subtask is executed, followed by the next highest priority value until the required resources are met for the task to be executed. At the same time, the status of all the satellite platforms assigned to the task is set to the working state until the end of the task processing, and then they are set to an idle state and can be reassigned to a new task.

The algorithm flow chart is shown in Figure 8.

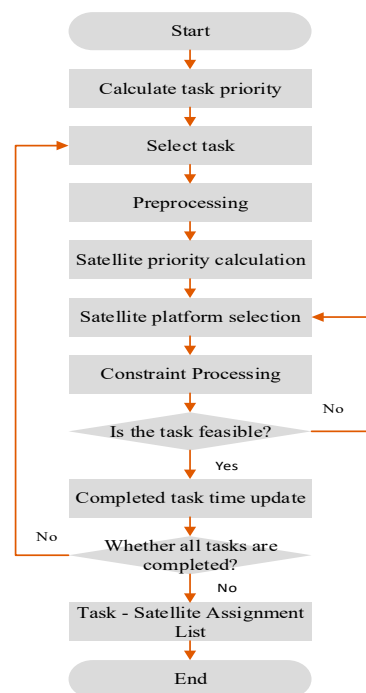


Figure 8. Constellation observation scheduling algorithm flow chart.

3.3. Observation Task Generation

Considering the influence of the various factors on the observation performance of space-based monitoring equipment, we designed an efficient optimal scheduling algorithm. It included the scheduling algorithm based on the priority of space objects and the scheduling algorithm based on the priority of the object update rate. It can realize the optimal scheduling of the observation tasks for a single satellite or a satellite constellation. A large number of space object orbit data are used for the numerical simulation analysis, and the analysis results verify the feasibility and adaptability of the scheduling method.

The observation task optimization algorithm we designed can create an observation plan for a single satellite or a constellation composed of multiple satellites at the same time. The observation objects can be set to prioritize the observation of key objects. The performance parameters of the satellite detectors can be set, and the number of observation satellites can be increased or reduced as needed.

The overall consideration for the optimization scheduling algorithm of the observation tasks is to observe as many objects as possible, and simultaneously make the rotation angle of each satellite switch smaller and observe the higher priority objects first. The priority of a single arc is higher than that of multiple arcs, considering the conditions of the sky, light, and Earth shadows, such as the Moon and the Sun.

4. Cataloging Requirements

The cataloging of space objects means that the monitoring network can continuously observe, match, correlate, and determine the orbits of space objects under normal operating conditions and can update the orbit information in a timely manner for each space object in the catalog. The number of space objects in the catalogue is an important index that reflects the ability of the monitoring network. The system performance is directly related to the number of space objects that are correctly cataloged.

The conditions for the space objects being judged to be correct for cataloging were as follows. The maximum observable time interval of LEO objects was about 24–48 h, the maximum observable time interval of GEO objects was about 48–168 h, and the maximum observable time interval of other space objects was less than 168 h. If the vast majority of LEO space objects can be observed every 24 h, the orbital cataloging for most LEO space objects can be achieved. In Section 5, the monitoring of space objects below 1000 km orbital altitude within 24 h on 26 February 2022 was calculated by the simulation, which was used to measure the cataloging ability of LEO space objects that were to be measured by the constellation.

The calculation process was as follows: (1) Calculate the observation time interval for each space object. (2) Calculate the maximum revisit time interval for each space object. (3) Calculate the maximum observation time interval distribution function for the entire set of observation objects. (4) Calculate the percentage of the time interval for cataloging space objects that are less than the value defined above.

5. Numerical Simulation Experiment

5.1. Experiment Overview

The simulation model of the detection equipment was established by comprehensively considering the aperture of the observation telescope and limiting the detection magnitude; space object orbit data; sky, light, and Earth shadow conditions; the space environment model; and atmospheric influence, etc. The number of space objects, arc segments, and detection frequencies that can be detected were numerically simulated and analyzed. The observation ability of the space objects with a different number of observation satellites and different constellation configurations was simulated and calculated. The number of objects and arcs that could be detected under each constellation configuration, as well as the distribution of the arc length and detection frequency, were analyzed, and the detection performance for several constellation configurations was compared.

The time of the simulation analysis was 26 February 2022, and the simulation duration was 24 h. The simulation was mainly for space objects with an orbital altitude less than 1000 km. It was assumed that the orientation of the detector on the satellite could be rotated according to the mission requirements during observation to realize the tracking and observation of space objects.

The simulation was mainly divided into two parts. The first part simulated and calculated the situation of the space objects passing through the detection range of the satellite detectors under different constellation configurations. That is, it analyzed the basic information, such as the number of objects and arcs, the arc length distribution, detectable

frequency, and so on in order to understand the influence of the orbital position of each constellation on the observation performance of the space objects. The second part was mainly based on the observation task scheduling algorithm of the space-based optical satellite constellation established above to allocate and schedule the observation tasks for the different constellation configurations. The various satellites in the constellation could coordinate, cooperate, and make full use of the observation resources and observation time. More space objects can be observed, and more observation data can be obtained, thereby providing support for the determination of the orbit of space objects and the establishment of a library of orbit catalogues of space objects.

For convenience, each constellation was numbered, as shown in Table 1.

Table 1. Constellation number table.

Constellation	Meaning
Constellation 1	12_3P, 12 satellites were evenly distributed on three orbital planes
Constellation 2	12_4P, 12 satellites were evenly distributed on four orbital planes
Constellation 3	12_6P, 12 satellites were evenly distributed on six orbital planes
Constellation 4	15_3P, 15 satellites were evenly distributed on three orbital planes
Constellation 5	15_5P, 15 satellites were evenly distributed on five orbital planes
Constellation 6	16_4P, 16 satellites were evenly distributed on four orbital planes
Constellation 7	18_3P, 18 satellites were evenly distributed on three orbital planes
Constellation 8	18_6P, 18 satellites were evenly distributed on six orbital planes
Constellation 9	20_5P, 20 satellites were evenly distributed on five orbital planes
Constellation 10	21_3P, 21 satellites were evenly distributed on three orbital planes
Constellation 11	24_3P, 24 satellites were evenly distributed on three orbital planes
Constellation 12	24_4P, 24 satellites were evenly distributed on four orbital planes
Constellation 13	24_6P, 24 satellites were evenly distributed on six orbital planes

5.2. Object Detectable Analysis

5.2.1. Detection Quantity Analysis

As shown in Figure 9, the observation performance of space objects varies greatly among the different constellation configurations, and the observation efficiency of the constellations 12_3, 12_4, and 12_6 that were composed of 12 satellites was relatively poor. Among them, the 12_3 constellation configuration meant that 12 satellites were evenly distributed on three orbital planes, and the right ascension of each orbital plane was 120 degrees different. The meaning of other constellation configurations can be deduced in the same manner.

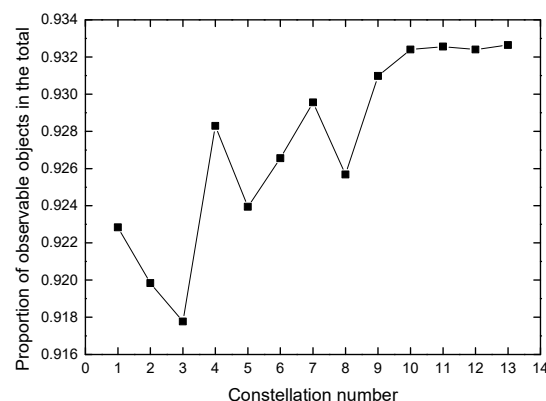


Figure 9. The proportion of space objects within the detectable range of the different constellation configurations to the total.

Secondly, the constellations composed of 15, 16, and 18 satellites had good monitoring performances, of which the observation performances of the 15_3 and 18_3 satellites were relatively good. In addition, the constellations composed of 20, 21, and 24 satellites had the

best performances and the largest numbers of observed targets. However, the larger the constellation size, the greater the cost. Therefore, the specific constellation to be selected for the space object observation should be comprehensively considered according to the demand and the cost.

5.2.2. Analysis of the Observation Arc Length

Figure 10 shows the relationship between the number of observable space objects in the different constellations and the length of the arcs. It can be seen that there were various arc lengths in the space objects observed by the different constellation configurations. For the same range of the detection arc length, the overall trend was that the more satellites the constellation has, the more space objects it can observe. However, for constellations with the same number of satellites, the monitoring efficiency was also slightly different due to the different constellation configurations. According to the post-processing requirements of the monitoring data, if the arc length was long, it was conducive to the determination of the space object orbit and the improvement in the accuracy.

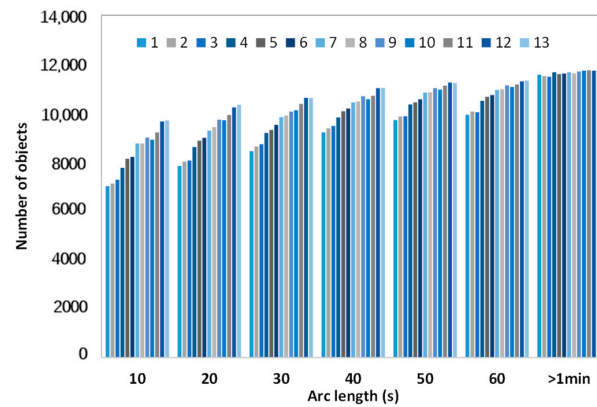


Figure 10. The distribution of observable objects with an arc length in the different constellation configurations.

Figure 11 shows the distribution of the number of arcs and arcs lengths observed in the different constellation configurations. It can be seen that the number of arcs corresponding to the different arc lengths was quite different. Among them, the number of arcs with arc lengths greater than 1 min was large, which was also conducive to improving the effectiveness of the observation data. Long observation arc lengths are preferred for space objects, which is conducive to data processing and the orbit determination of space objects. When the arc length was less than 1 min, it can be seen from the above figure that the number of arcs corresponding to the arc length gradually increased from 10 s to 60 s. For the same arc length range, for example, when the arc length was approx. 40 s, the larger the constellation size, the more arc segments could be observed.

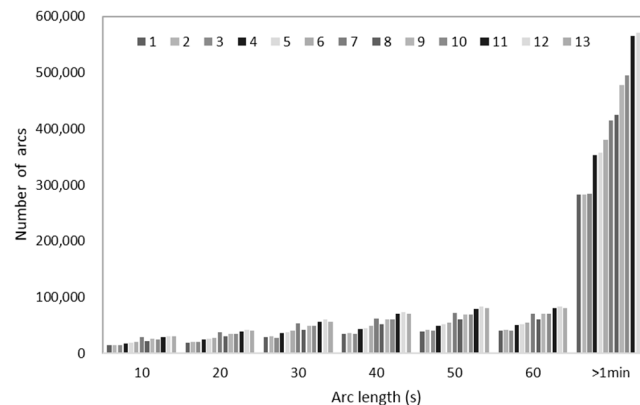


Figure 11. Observable arc length distribution of the different constellation configurations.

5.2.3. Observation Frequency

Figure 12 shows the relationship between the number of observable space objects in the different constellations and the detectable frequency of these objects. As can be seen from the figure, for the constellations with a small number of satellites, the detectable frequency for most space objects was approx. 30–50 times. For large-scale constellations with more satellites, the detectable frequency of space objects increased considerably by approx. 70–80 times. Therefore, the larger the constellation size, the more observation opportunities, and the easier it is to observe the key targets.

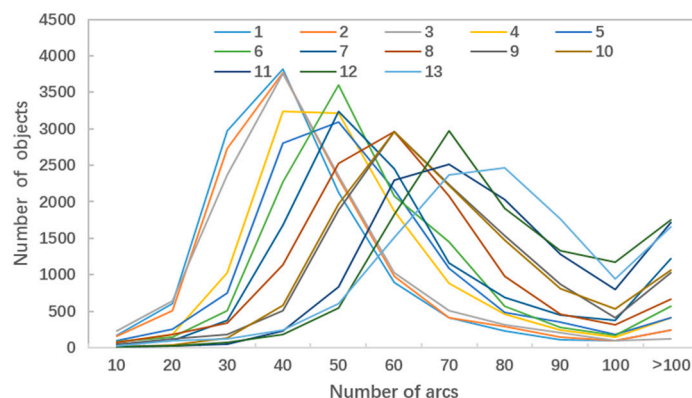


Figure 12. Variation of the number of objects observed using the different constellation configurations for the observation frequency.

5.3. Tacking Observation Performance

Based on the optimal scheduling algorithm of the satellite constellation observation tasks designed above, the monitoring ability of the different constellation configurations for LEO space objects was simulated, mainly for space objects with orbital altitudes less than 1000 km. The simulation conditions were that each object was observed for at least 60 s, and the switching time of the satellite detectors was 5 s. The field of view of the telescope was 15° , the maximum observation distance was 1000 km, and the simulation duration was 24 h.

It can be seen from Figure 13 that the fourth, seventh, and eleventh constellation configurations had good tracking observation performances. The corresponding constellation configurations were 15_3, 18_3, and 24_3, respectively. They tracked 91.10%, 91.77%, and 92.75% of LEO space objects, respectively, within 24 h. If they were observed continuously every day, most LEO space objects could be catalogued. Among these constellation configurations, 15_3 and 18_3 were the locally optimal constellation configurations, and the 24_3 constellation was the globally optimal constellation configuration. However, for the constellations composed of 15 and 18 satellites, the number of satellites was less than the 24-satellite constellation, resulting in a lower cost and a higher cost performance. The specific constellation configuration can be determined according to the needs of the users.

In Figure 14, the 15_3 constellation configuration was taken as an example, to analyze the number of space objects that could be observed by each satellite in the constellation under the observation task optimization scheduling algorithm. Here, 15_3 indicated that the constellation was composed of 15 satellites, which were evenly distributed on three orbital planes, and the right ascension of each orbital plane was evenly distributed. The detector on the satellite could rotate freely, so that it could observe the specified space objects. The number of space objects that could be observed by each satellite in the constellation within 24 h is shown in the above figure. It can be seen that the number of space objects that can be tracked by most satellites was more than 800, and the number of objects that can be tracked by a few satellites was approx. 650. The constellation tracked and observed 11,522 objects in 24 h, accounting for 91.10% of the total objects participating in the simulation. It had a

good observation efficiency. If the constellation continued to observe space debris every day, it could catalog most space objects with an orbital height of less than 1000 km.

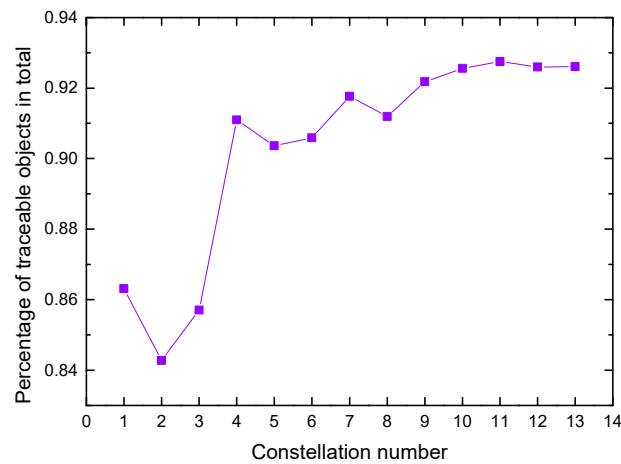


Figure 13. Proportion of objects that can be tracked within 24 h in the different constellation configurations.

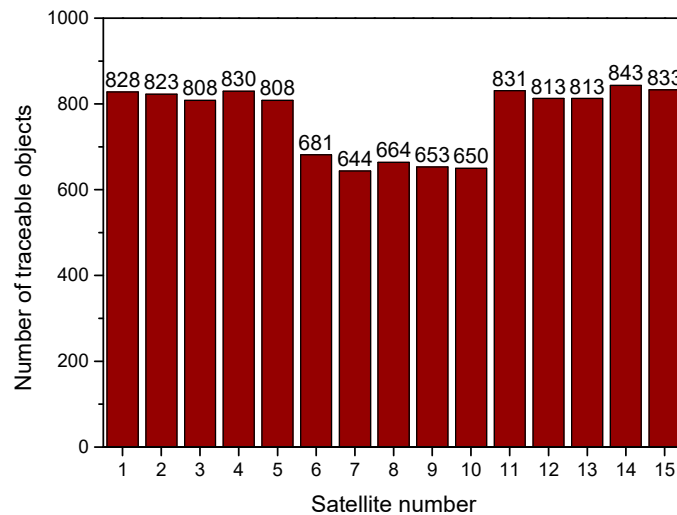


Figure 14. The number of objects that could be tracked by each satellite in the 15_3 constellation in 24 h.

6. Conclusions

In this paper, a mathematical model of a constellation design was established by considering various factors, and was optimized by using a genetic algorithm to obtain the optimal orbital height of 609.782 km, the optimal orbital inclination angle of 96.142°, and a high-quality constellation configuration, which was mainly used to observe space objects with an orbital altitude below 1000 km. A greedy algorithm based on a multi-dimensional list was designed to optimize the scheduling of the constellation observation tasks and realize the optimization of the single-satellite observation tasks and constellation observation tasks. Through the simulation experiments, the mathematical model and the optimization algorithm established above were verified.

It was found that the constellation composed of 15 satellites had a high cost performance, achieved a high observation efficiency with relatively few satellites, and tracked 91% of the objects with an orbital altitude of less than 1000 km every 24 h. The constellation composed of 24 satellites distributed on three orbital planes had the best observation efficiency. It tracked approx. 93% of LEO orbit objects in 24 h. Through long-term continuous observation, these constellations could maintain an orbit catalogue of most low orbit objects, identify dangerous rendezvous times, and prevent the loss of space assets.

Author Contributions: Conceptualization, G.L.; methodology, G.L., J.L. and H.J.; software, G.L.; validation, G.L., J.L. and H.J.; writing—original draft preparation, G.L.; writing—review and editing, G.L., J.L., H.J. and C.L.; supervision, J.L., H.J. and C.L.; project administration, J.L.; funding acquisition, J.L. and H.J. All authors have read and agreed to the published version of the manuscript.

Funding: This research was funded by the Space Debris Research Project of China (No. KJSP2020020201, No. KJSP2020020202), the China National Key R&D Program during the 14th Five-year Plan Period (No. 2022YFC2807304), and the Foundation Laboratory of Pinghu (No. 2020AB01001).

Institutional Review Board Statement: Not applicable.

Informed Consent Statement: Not applicable.

Data Availability Statement: Not applicable.

Conflicts of Interest: The authors declare no conflict of interest.

References

1. Klinkrad, H. *Space Debris: Models and Risk Analysis*; Springer: New York, NY, USA, 2006.
2. Olmedo, E.; Sanchez-Ortiz, N. Space debris cataloguing capabilities of some proposed architectures for the future European space situational awareness system. *Mon. Not. R. Astron. Soc.* **2010**, *403*, 253–268. [[CrossRef](#)]
3. Riot, V.; de Vries, W.; Simms, L.; Bauman, B.; Carter, D.; Phillion, D.; Olivier, S. The Space-based Telescopes for Actionable Refinement of Ephemeris (STARE) mission. In Proceedings of the 27th Annual AIAA/USU Conference on Small Satellites, Logan, UT, USA, 10–15 August 2013.
4. Li, G.; Liu, J.; Cheng, H. Space Debris Laser Ranging Technology and Applications. *Space Debris Res.* **2020**, *20*, 40–48.
5. Cui, Z.; Xu, Y. Impact simulation of Starlink satellites on astronomical observation using worldwide telescope. *Astron. Comput.* **2022**, *41*, 100652. [[CrossRef](#)]
6. Julian, R.; Emiliano, C.; Thomas, S. The stare and chase observation strategy at the Swiss Optical Ground Station and Geodynamics Observatory Zimmerwald: From concept to implementation. *Acta Astronaut.* **2021**, *189*, 352–367.
7. Lawrence, A.; Rawls, M.L.; Jah, M.; Boley, A.; Di Vruno, F.; Garrington, S.; McCaughrean, M. The case for space environmentalism. *Nat. Astron.* **2022**, *6*, 428–435. [[CrossRef](#)]
8. Ravago, N.; Jones, B.A. Risk-aware sensor scheduling and tracking of large constellations. *Adv. Space Res.* **2021**, *68*, 2530–2550. [[CrossRef](#)]
9. Steindorfer, M.A.; Kirchner, G.; Koidl, F.; Wang, P.; Jilete, B.; Flohrer, T. Daylight space debris laser ranging. *Nat. Commun.* **2020**, *11*, 3735. [[CrossRef](#)]
10. Pierre, B.; Marc, D.; Georges, Z. Large satellite constellations and space debris: Exploratory analysis of strategic management of the space commons. *Eur. J. Oper. Res.* **2022**, *304*, 1140–1157. [[CrossRef](#)]
11. Li, G.; Jiang, H.; Cheng, H.; Liu, J. Research on monitoring effectiveness of optical satellite constellation. In Proceedings of the 68th International Astronautical Congress (IAC), Adelaide, Australia, 25–29 September 2017.
12. Ma, B.; Shang, Z.; Hu, Y.; Hu, K.; Wang, Y.; Yang, X.; Jiang, P. Night-time measurements of astronomical seeing at Dome A in Antarctica. *Nature* **2020**, *583*, 771–774. [[CrossRef](#)]
13. Huang, Y.; Mu, Z.; Wu, S.; Cui, B.; Duan, Y. Revising the Observation Satellite Scheduling Problem Based on Deep Reinforcement Learning. *Remote Sens.* **2021**, *13*, 2377. [[CrossRef](#)]
14. Silha, J.; Schildknecht, T.; Hinze, A.; Flohrer, T.; Vananti, A. An optical survey for space debris on highly eccentric and inclined meo orbits. *Adv. Space Res.* **2017**, *59*, 181–192. [[CrossRef](#)]
15. López-Casado, C.; Pérez-del-Pulgar, C.; Muñoz, V.F.; Castro-Tirado, A.J. Observation scheduling and simulation in a global telescope network. *Future Gener. Comput. Syst.* **2019**, *95*, 116–125. [[CrossRef](#)]
16. Ip, A.W.; Xhafa, F.; Dong, J.; Gao, M. Chapter 6—An overview of optimization and resolution methods in satellite scheduling and spacecraft operation: Description, modeling, and application. In *Aerospace Engineering, IoT and Spacecraft Informatics*; Elsevier: Amsterdam, The Netherlands, 2022; pp. 157–217; ISBN 9780128210512.
17. Jing, L.; Hong, C. Deployment and Performance Analysis of Early-Warning Satellite Based on STK. *Shipboard Electron. Countermeas.* **2012**, *35*, 1–4.
18. Wang, C.; Chen, X.; Deng, Y. Infrared LEO Constellation Design by GDE 3 Algorithm. *J. Beijing Univ. Aeronaut. Astronaut.* **2010**, *36*, 857–862.
19. Zhang, R.; Tu, R.; Zhang, P.; Liu, J.; Lu, X. Study of satellite shadow function model considering the overlapping parts of Earth shadow and Moon shadow and its application to GPS satellite orbit determination. *Adv. Space Res.* **2019**, *63*, 2912–2929. [[CrossRef](#)]
20. Zhang, S.; Zhu, Z.; Hu, H.; Li, Y. Research on Task Satellite Selection Method for Space Object Detection LEO Constellation Based on Observation Window Projection Analysis. *Aerospace* **2021**, *8*, 156. [[CrossRef](#)]
21. Guan, M.; Xu, T.; Gao, F.; Nie, W.; Yang, H. Optimal Walker Constellation Design of LEO-Based Global Navigation and Augmentation System. *Remote Sens.* **2020**, *12*, 1845. [[CrossRef](#)]

22. Jia, L.; Zhang, Y.; Yu, J.; Wang, X. Design of Mega-Constellations for Global Uniform Coverage with Inter-Satellite Links. *Aerospace* **2022**, *9*, 234. [[CrossRef](#)]
23. Zhang, Y.; Fan, L.; Zhang, Y.; Xiang, J.H. *Theory and Design of Satellite Constellations*; Science Press: Beijing, China, 2008.
24. Hu, M.; Ruan, Y.; Zhou, H.; Xu, J.; Xue, W. Long-Term Orbit Prediction and Deorbit Disposal Investigation of MEO Navigation Satellites. *Aerospace* **2022**, *9*, 266. [[CrossRef](#)]
25. Yasini, T.; Roshanian, J.; Taghavipour, A. Improving the low orbit satellite tracking ability using nonlinear model predictive controller and Genetic Algorithm. *Adv. Space Res.* **2023**, *71*, 2723–2732. [[CrossRef](#)]
26. Orbital Debris Quarterly News. National Aeronautics and Space Administration. Volume 26, Issue 1; March 2022. Available online: <https://orbitaldebris.jsc.nasa.gov> (accessed on 12 August 2022).
27. Chen, X.; Reinelt, G.; Dai, G.; Wang, M. Priority-based and conflict-avoidance heuristics for multi-satellite scheduling. *Appl. Soft Comput.* **2018**, *69*, 177–191. [[CrossRef](#)]
28. Ben-Larbi, M.K.; Pozo, K.F.; Haylok, T.; Choi, M.; Grzesik, B.; Haas, A.; Krupke, D.; Konstanski, H.; Schaus, V.; Fekete, S.P.; et al. Towards the automated operations of large distributed satellite systems. Part 1: Review and paradigm shifts. *Adv. Space Res.* **2021**, *67*, 3598–3619. [[CrossRef](#)]
29. Liu, Y.; Zhang, S.; Hu, H. A conflict avoidance algorithm for space-based collaborative stereo observation mission scheduling of space debris. *Adv. Space Res.* **2022**, *70*, 2302–2314. [[CrossRef](#)]
30. Chang, Z.; Chen, Y.; Yang, W.; Zhou, Z. Mission planning problem for optical video satellite imaging with variable image duration: A greedy algorithm based on heuristic knowledge. *Adv. Space Res.* **2020**, *66*, 2597–2609. [[CrossRef](#)]
31. Qu, G.; Brown, D.; Li, N. Distributed Greedy Algorithm for Satellite Assignment Problem with Submodular Utility Function**The work is supported by Lincoln Laboratory with award #7000292526. *IFAC-PapersOnLine* **2015**, *48*, 258–263. [[CrossRef](#)]

Disclaimer/Publisher’s Note: The statements, opinions and data contained in all publications are solely those of the individual author(s) and contributor(s) and not of MDPI and/or the editor(s). MDPI and/or the editor(s) disclaim responsibility for any injury to people or property resulting from any ideas, methods, instructions or products referred to in the content.